LAWRENCE
LIVERMORE
NATIONAL
LABORATORY

LLNL-JRNL-404604

Optical Transmission of Glass for the National Ignition Facility Near Backscatter Imagers Under X-Ray Exposure

R. A. London, D. H. Froula, C. M. Sorce, J. D. Moody, L. J. Suter, S. H. Glenzer, O. S. Jones, N. B. Meezan, M. D. Rosen

June 11, 2008

Review of Scientific Instruments

Disclaimer

Optical Transmission of Glass for the National Ignition Facility Near Backscatter Imagers Under X-Ray Exposure

R. A. London, D. H. Froula, C. M. Sorce, J. D. Moody, L. J. Suter, S. H. Glenzer, O. S. Jones, N. B. Meezan, and M. D. Rosen

Lawrence Livermore National Laboratory, 7000 East Avenue, Livermore, CA 94550

Abstract. In experiments at the National Ignition Facility, the near backscatter imager materials need to maintain high optical transmission while exposed to hohlraum generated x rays. Glass plates are incorporated in the design to protect the optical scattering plates from x-ray damage. Radiation environments spanning those expected on NIF have been produced at the Omega Laser Facility by symmetric laser illumination of 1-mm sized gold spheres. The time-dependent ultra-violet transmission of sample glass plates was measured. The data is interpreted with a free electron absorption model. Combined with simulations of the hohlraum x-ray emission, this model is used to predict the transmission of the glass plates on the NIF. We predict that the plates should perform adequately up to the peak of the laser pulse.

I. Introduction.

At the National Ignition Facility (NIF)[1], the light backscattered from laser-produced plasmas will be measured on two of the 48 laser quads using full aperture backscatter stations[2] and near backscatter imagers[3]. Measurements will be made in two wavelength bands distinguished by their respective scattering processes, 351-353 nm for stimulated Brillouin scattering (SBS) and 450-750 nm for stimulated Raman scattering (SRS). Each near backscatter imager measures light scattered outside the aperture of the focusing lens using a Lambertian scattering plate mounted on the target chamber wall. A gated charge coupled device is used to image the scatter plate and measure the total energy[4].

The near backscatter imager (NBI) scattering plates are to be made of Spectralon® (Labsphere) a material composed of pressed polytetrafluoroethene (i.e. Teflon®). Spectralon® is a very efficient (99%), nearly Lambertian scatterer over the necessary wavelength band. However, it is susceptible to melting and/or photo-chemical damage[5] by x rays emitted by ignition scale hohlraums. Therefore, we plan to cover the scattering plates with SiO_2 glass plates to protect them from x-ray damage ("x-ray shields"). With a melting temperature of 1775 K, glass is much less susceptible to damage. The x-ray shields must be approximately 10 μm thick to absorb 99% of the expected x rays, but in reality they will be much thicker for structural integrity. Ideally, the shields should have only a small and well-characterized optical loss.

A remaining question is whether x-ray irradiation of the glass shields will reduce their transmission of the backscattered laser light, leading to a reduced, and more importantly, uncertain efficiency of the NBI system. In order to answer this question, we have performed experiments at the Omega Laser Facility at the Laboratory for Laser Energetics studying the real-time transmission of glass plates exposed to x rays of similar spectrum and flux to those expected at the National Ignition Facility. We interpret the data with a model for x-ray induced absorption in the glass. This model is then used to predict the behavior of the x-ray shields at NIF.

II. Experiment

The transmission of the samples was measured using a relatively low energy (<85J) 351-nm probe beam. Figure 1 shows the experimental setup where the probe beam passed through the 3-mm thick samples placed 60-cm from target chamber center. An uncoated fused silica spherical mirror reflected 4% of the incident light back through the sample and onto a calorimeter and a fiber optic cable located on a diagnostic platform just outside the chamber. The fiber optic cable transported the light to a streak camera. This system was configured to have a <50 ps temporal resolution. A second fiber optic cable collected light incident from the probe beam. This light was coupled into the same streak camera providing an incident pulse shape. The temporally resolved transmission was measured by dividing the incident and the transmitted powers.

An x-ray source was produced by 54 laser beams of 351 nm wavelength, incident on 1-mm Au spheres[6]. The x-ray power was measured on each shot using an absolutely calibrated soft x-ray spectrometer DANTE[7]. The maximum x-ray power was achieved using laser pulses 1-ns long with a total laser energy of 25 kJ, while the minimum was produced using 3-ns long laser pulses with 9.5 kJ of energy. Table 1 summarizes the experimental parameters.

Table 1. Omega Experimental Parameters and Data Summary

Laser Energy (kJ)	Pulse length (ns)	x-ray fluence* (J/cm^2)	Maximum absorption (%)
9.5	3	0.10	0 – 10
25	1	0.28	15 – 25

* The x-ray fluence is taken at end of laser pulse.

Figure 2(a) shows the measured incident and transmitted probe pulses for the low power shot (9.5 kJ in 3 ns). The x-ray flux on the sample and the UV transmission are shown in Figure 2(b). This is the transmission for two-passes through the plate. No measurable absorption throughout the 3-ns experiment is observed. Taking into account measurement uncertainties, we conclude that the absorption lies between 0 and 10% in this case. Figure 2(c) shows highest x-ray power results where the transmission begins to decrease at 0.7 ns, when the fluence has reached 0.12 J/cm^2. Near the end of the laser pulse, the transmission is reduced to 80±5%. The maximum measured absorption for each experiment is listed in Table 1.

III. Model for absorption and predictions for NIF

Previous work has shown that x-ray irradiation can alter the optical properties of transparent materials by creating free electrons, above the band gap of the material[8]. The important quantity for the NBI plates is the imaginary part of the index, giving rise to absorption. We extend the model Theobald et al.[8] to include a specific description of free electron generation.

The ultraviolet/optical (abbreviated as UV) absorption coefficient is modeled by the Drude formula[9]:

$$(1) \qquad \kappa_{uv} = \frac{\nu}{\eta c}\left(\frac{\omega_p}{\omega}\right)^2 \frac{1}{1+\left(\nu/\omega\right)^2},$$

where ν is the electron collisional rate, η the index of refraction of the un-irradiated material, ω_p the plasma frequency ($\propto n_e^{1/2}$ where n_e is the electron density), and ω the

optical angular frequency. The transmission of a slab at normal incidence is $T = \exp(-\tau_{uv})$, where $\tau_{uv} = \int \kappa dz$, is the optical depth, z being the depth into the material.

Assuming that the collisional rate is constant we integrate Eq. (1) to find the optical depth:

$$(2) \qquad \tau_{uv} = 1.99 \ \nu_{15}\left(\lambda_{\mu m}\right)^2 N_{e17} \frac{1}{1 + 0.28 \ \left(\nu_{15}\lambda_{\mu m}\right)^2},$$

where ν_{15} is the collision rate in units of 10^{15} Hz, $\lambda_{\mu m}$ is the wavelength in μm, N_{e17} is the electron column density ($\int n_e dz$) in units of 10^{17} cm^{-2}, and we have assumed $\eta = 1.5$.

The electron density is modeled by a time-dependent rate equation:

$$(3) \qquad \frac{dn_e}{dt} = P(t) - \frac{n_e}{t_r},$$

where P(t) is the net ionization rate per unit volume and t_r is the recombination time.

Ionization is caused directly by x rays and by a cascade of Auger and collisional processes that follow each photo ionization event. Previous work indicates that each cascade takes place in less than ~100 fs[10] and produces a number of electrons equal to the x-ray energy divided by a creation energy, ε, typically 2-3 times the band gap.[11] For SiO_2, both experiment and theory indicate that ε ≈ 18 eV.[12, 13] Since the timescale for the photoelectron cascade is much shorter than the x-ray pulses of interest (of order ns) and the electron ranges are short, we assume that each absorbed x ray instantly and locally generates a number of electrons equal to its energy divided by ε. For example, a 1 keV photon absorbed in SiO_2 would generate about 56 electrons.

Defining a local x-ray dose-rate, δ, as the energy absorbed per unit volume per unit time, we write the ionization rate as $P\left(z\right) = \delta\left(z\right)/\varepsilon$. Using this expression and assuming a flattop pulse, we integrate Eq. (3) to find:

$$(4) \qquad N_e = \frac{n_a t_r}{\varepsilon}\left(1 - e^{-t/t_r}\right) \int \delta dz.$$

The x-ray dose rate is given by $\delta(z) = \int \alpha(\nu) F_\nu(z) d\nu$, where α(ν) is the frequency dependent x-ray absorption coefficient, assumed constant in time and space, and F_ν is the specific x-ray flux (power per unit area per unit frequency). Since x-ray scattering is weak, the flux at each frequency decreases exponentially with depth: $F_\nu\left(z\right) = F_\nu\left(0\right)e^{-\alpha z}$.

The column density can now be expressed in terms of the x-ray fluence, F, defined as the time and frequency integral of the flux:

$$(5) \qquad N_e = \frac{F}{\varepsilon}\frac{t_r}{t}\left(1 - e^{-t/t_r}\right) \ .$$

We note that the frequency dependences of the x-ray spectrum and absorption coefficient drop out of the expression for N_e. This occurs for plates much thicker than the longest x-ray mean-free path, as is the case here.

Combining Eqs. (2) and (5) we get:

$$(6) \qquad \tau_{uv} = 4.60 \ \ \nu_{15}\left(\lambda_{\mu m}\right)^2 \frac{F}{\varepsilon/18}\left[\frac{t_r}{t}\left(1 - e^{-t/t_r}\right)\right]\left[1 + 0.28 \ \left(\nu_{15}\lambda_{\mu m}\right)^2\right]^{-1}$$

Research on hot carrier dynamics and short pulse optical laser interaction with SiO_2 gives some information on the values of the parameters in our model. Collision rates determined by that work range from 10^{14} to 10^{16} Hz.[14,15] The recombination time is less certain. With ultra-short laser excitation (~100 fs), decay times for excited electrons of around 150 fs have been observed.[15,16,17] This decay process has been attributed primarily to the formation of self-trapped excitons. However, these ultra-short decay times have been observed only for low electron creation densities (~10^{19} cm^{-3}). It is likely that the self-excited exciton trapping mechanism saturates for the higher creation densities of interest here (~10^{21} cm^{-3}). In that case, the appropriate timescale would be the true recombination timescale, which may be in the ns realm. Owing to the uncertainty in the values of ν and t_r, we treat them as free parameters within the limits mentioned above, and fit them to our experimental data.

We compare results of the model described above to the observed transmission data, listed in Table 1. We thereby find the region of the (ν-t_r) parameter space wherein the model agrees with the data, as shown in Figure 3a. The dominant constraints on the parameters are placed by the data from the high-energy shot. The data from the low-energy shot place an upper limit on t_r that is consistent with the high-energy data, but which do not further constrain the parameters. The acceptable values of ν range from 0.4 to 10x10^{15}Hz, while t_r ranges from 0.15 to 10 ns. Within this region, t_r primarily decreases as ν increases.

Having determined the range of model parameters that fit the Omega experiments, we now estimate the absorption expected for the NIF x-ray shields. We use calculations of the x-ray flux based on simulations of ignition hohlraums performed with the HYDRA radiation-hydrodynamics code.[18] More information about NIF target designs is given in recent papers.[19,20] The flux at the angular position of the NIF NBI plates (30º from the hohlraum axis and 5 m away) was simulated with a ray tracing code. Calculations were done for both a small hohlraum irradiated by 96-beams and a large hohlraum irradiated by 192-beams. The relevant parameters of these targets are given in Table 2. The spectra

for both cases are characterized by a broad peak at about 1 keV photon energy and a FWHM of 1 keV. The attenuation length for 1 keV photons in SiO_2 is 1.4 μm.

We use the fluences and pulse lengths predicted for NIF targets to calculate the expected UV and optical absorption. We first discuss the response to the full duration of the x-ray pulses. Although the pulse profiles are somewhat more complicated for the NIF cases, we approximate them as square profiles to maintain the simple UV absorption formula used for the Omega experiments, i.e. Eq. (6). The duration of each square pulse is chosen to give the same fluence and peak flux as the simulated pulses. This level of accuracy is consistent with the other approximations made in the model. Figure 3b shows the expected UV absorption at 351 nm for the NIF 192 beam case, over the whole range of allowed model parameters determined from the Omega data. The limiting range of absorption values for both 96 and 192 beam experiments is shown in Table 2.

Table 2. NIF Hohlraum parameters and predicted absorptivities

Number of beams	Hohlraum Dimensions (mm)	Laser energy (kJ)	x-ray FWHM (ns)	x-ray fluence (J/cm^2)	Absorption range (%)
96	3.6 x 6.4	380	3.0	0.074	1.4–6.7
192	5.1 x 9.1	950	3.7	0.13	2.0–11

The maximum absorption expected at NIF at 351 nm is 11%. This value is sufficiently small to maintain the desired accuracy of the backscattered energy measurement. The situation is expected to be even better, since the peak of the laser pulse, when the maximum backscatter is expected, occurs about 1 ns before the peak of the x-ray pulse. At this time, the x-ray fluence is only 1/3 of the full value and maximum predicted absorption at 351 nm is only 4 %.

We have also looked at predictions for the optical (SRS) band. The absorption scales approximately as λ^2 in the SRS band. At the longest wavelength (750 nm–the worst case) the absorption is predicted to be in the range of 2 to 40% for 192 beam experiments. The maximum value of 40%, although not likely in the context of the model, would be unacceptably large. However, at the peak of the laser pulse, the maximum absorption at 750 nm is only 16%.

IV. Conclusions.

We have measured the reduction in UV transmission of SiO_2 glass plates exposed to x-ray pulses to be 15-25% for an x-ray fluence of 0.28 J/cm^2. Combining a model for x-ray induced absorption with radiation-hydrodynamics simulations of NIF targets, we predict the reduction in transmission expected for the NBI x-ray shields. We find that the reduction is less that 11% for wavelengths near 351 nm, where SBS occurs. This is sufficiently small to maintain the desired accuracy of the NBI for SBS. At the maximum

wavelength for SRS measurements, 750 nm, the absorption is expected to be higher. At the peak of the laser pulse, when backscatter is expected to be strongest, the absorption at all wavelengths is predicted to be less than 16%. Future experiments with improved measurement accuracy and at longer wavelengths, up to 750 nm, would reduce the uncertainties in the absorption estimates for the NIF NBI shields.

Acknowledgements

We thank O. L. Landen for helpful comments on the manuscript. This work performed under the auspices of the U.S. Department of Energy by Lawrence Livermore National Laboratory under Contract DE-AC52-07NA27344.

Figure Captions

Figure 1. This schematic diagram of the experimental layout at the Omega Laser Facility shows the glass sample as a vertical dashed line segment in front of the spherical mirror on the right. The 1-mm diameter gold sphere is irradiated by 54 beams and emits nearly isotropic x rays. The 351-nm probe beam passes through the sample twice. The transmitted beam and a reference picked off from B30 are relayed to a streak camera via optical fibers.

Figure 2. Panels (a) and (c) show the time-resolved incident (dashed) and (2-pass) transmitted (solid) 351-nm powers, in relative units. Panels (b) and (d) show the 2-pass transmission of the sample (black), and the x-ray fluence at the sample. The top panels (a) and (b) are for the 9.5 kJ/3 ns shot, while the bottom panels are for the 25 kJ/1 ns shot.

Figure 3. Panel (a) shows the recombination time–collisional rate (t_r–ν) parameter space for the absorption model, as constrained by the Omega data. The curve labeled "low-10%" gives the values that produce 10% absorption for the low-energy shot. All values below and to the left of this curve are consistent with the low-energy data. The "high-15%" and "high-25%" curves correspond to the minimum and maximum absorption values consistent with the high-energy shot data. The filled region shows the range of values of t_r and ν allowed by the Omega data. Panel (b) shows the predicted 351-nm absorption values of SiO_2 x-ray shields for 1MJ, 192 beam NIF hohlraum shots, using the parameter constraints shown in panel (a). The lines and shading are the same as for panel (a). The range of predicted absorption values is 2-11 %.

Figure 1.

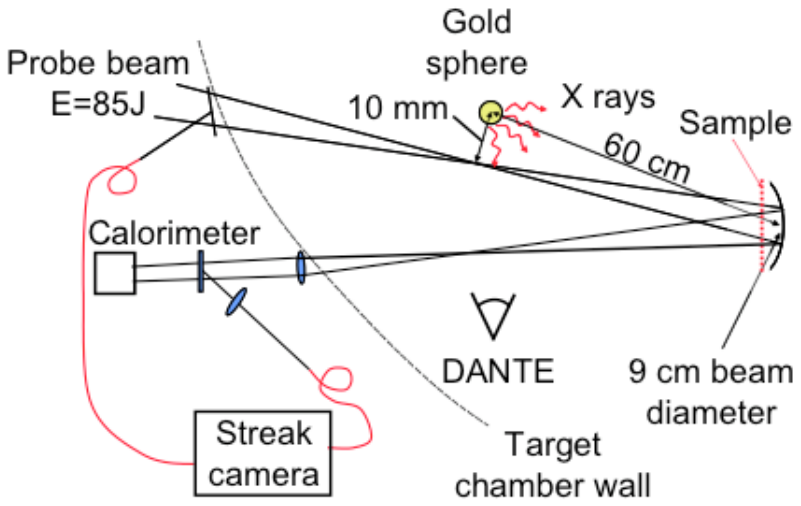

Figure 2

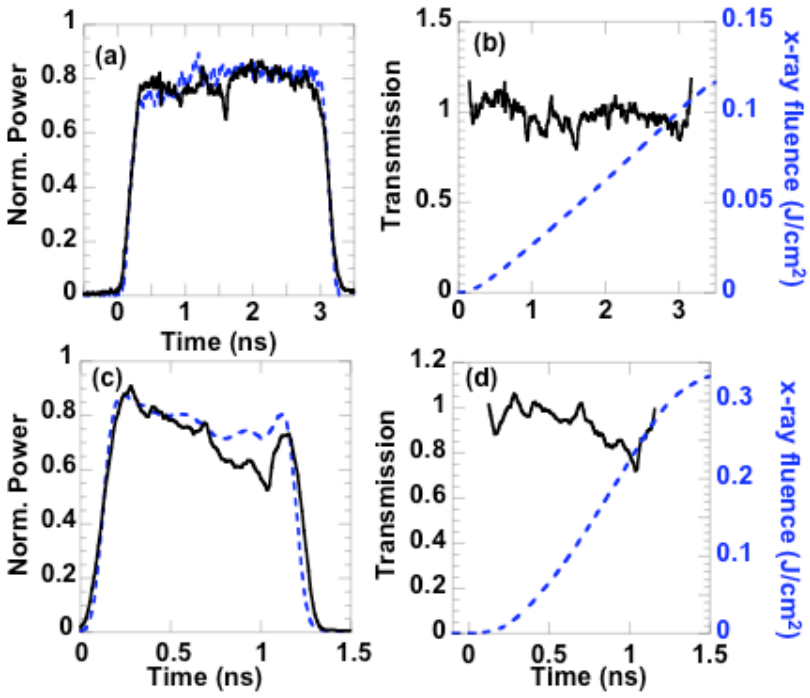

Figure 3

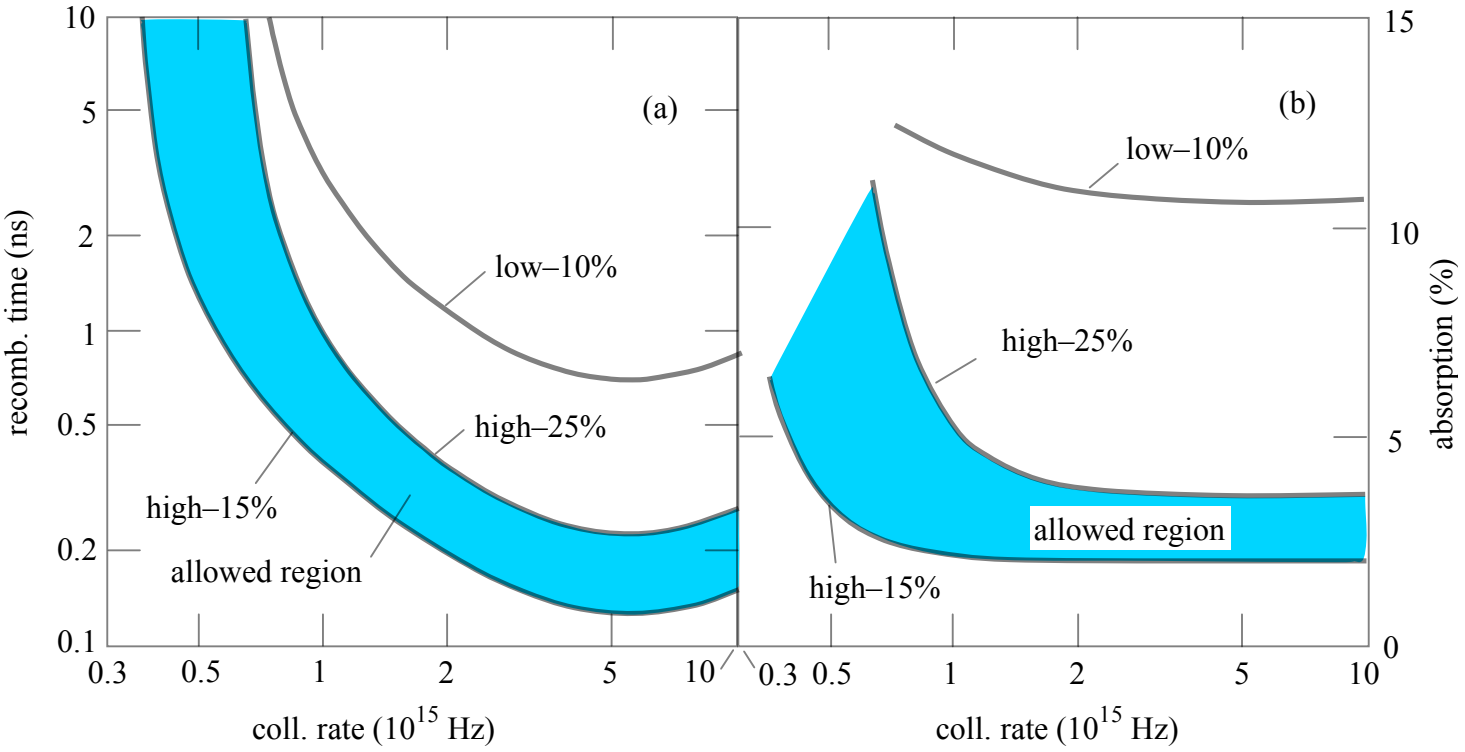
recomb. time (ns)
10
5
2
1
0.5
0.2
0.1
(a)
low–10%
high–25%
high–15%
allowed region
0.3
0.5
1
2
5
10
coll. rate (10^{15} Hz)
(b)
low–10%
high–25%
allowed region
high–15%
15
10
5
0
absorption (%)

References

[1] E. Moses et. al., Fusion Science Tech. **47**, 314 (2005).

[2] D. H. Froula et.al., Rev. Sci. Instrum. **75,** 4168 (2004).

[3] A. R. MacKinnon et.al., Rev. Sci. Instrum. **77,** 10E529 (2006).

[4] S. H. Glenzer et. al., Nature **3**, 716 (2007).

[5] Y. Zhang, Adv. Polym. Sci. **168**, 291 (2004).

[6] E. L. Dewald, M. Rosen, S. H. Glenzer, L. J. Suter, F. Girard, J. P. Jadaud, J. Schein, C. Constantin, P. Neumayer and O. L. Landen, Phys. Plasmas, in press (2008).

[7] C. Sorce et.al., Rev. Sci. Instrum. **77**, 10E518 (2006).

[8] W. Theobald, J. E. Miller, T. R. Boehly, E. Vianello, D. D. Meyerhofer, T. C. Sangster, J. Eggert and P. M. Celliers, Phys. Plasmas **13**, 122702 (2006).

[9] For example: J. D. Jackson, *Classical Electrodynamics, 2nd Edition*, (Wiley: New York, 1975), p. 284-288.

[10] B. Ziaja, R. A. London, and J. Hajdu, J. App. Phys. **97**, 064905-1 (2005).

[11] F. S. Goulding and Y. Stone, Science, **170**, 280 (1970).

[12] G. A. Ausman and F.B. McLean, Appl. Phys. Lett. **26,** 173 (1975).

[13] R. C. Alig, S. Bloom, and C. W. Struck, Phys. Rev. B **22**, 5565 (1980).

[14] D. Arnold and E. Cartier, Phys. Rev. B. **45**, 102 (1992).

[15] Q. Sun, et al., Front. Phys. China, **1**, 67 (2006).

[16] P. Audebert et al., Phys. Rev. Lett. **73**, 1990 (1994).

[17] G. Petite, P. Daguzan, S. Guizard, P. Martin, App. Surf. Sci. **109/110**, 36 (1997).

[18] M. Marinak et al., Phys. Plasmas **5**, 1125 (1998).

[19] S. W. Haan et al., Eur. Phys. J. D **44**, 249 (2007).

[20] D. A. Callahan, et al., Proc. Int. Conf. on Inertial Fusion Sci. and App., in press (2008).